

# Potential and current distribution in strongly anisotropic $\text{Bi}_2\text{Sr}_2\text{CaCu}_2\text{O}_8$ single crystals at current breakdown

I. Pethes,<sup>1</sup> Á. Pallinger,<sup>1</sup> B. Sas,<sup>1</sup> G. Kriza,<sup>1</sup> K. Vad,<sup>2</sup> A. Pomar,<sup>3</sup> F. Portier,<sup>3</sup> and F. I. B. Williams<sup>3</sup>

<sup>1</sup>Research Institute for Solid State Physics and Optics, PO Box 49, H-1525 Budapest, Hungary

<sup>2</sup>Institute of Nuclear Research, PO Box 51, H-4001 Debrecen, Hungary

<sup>3</sup>Service de Physique de l'Etat Condens, Commissariat l'Energie Atomique, Saclay, F-91191 Gif-sur-Yvette, France

(Dated: August 13, 2002)

Experiments on potential drops in the low temperature vortex solid phase of monocrystalline platelets of superconducting  $\text{Bi}_2\text{Sr}_2\text{CaCu}_2\text{O}_8$  (BSCCO) subjected to currents driven either through an *ab* surface or from one such surface to another show evidence of a resistive - non resistive front moving progressively out from the current contacts as the current increases. An experiment has been carried out to detect the position of the front with depth. The position of the front associated with the injection point appears to depend only on the current magnitude and not on its withdrawal point. This is the result of simultaneous *ab* and *c* current resistive breakdown for which we present a model which leads to a wedge like resistive front. Measurements in *ab* or *c* configurations give the same information which involves both *ab* and *c* properties.

PACS numbers: 74.72.Hs, 74.25.Fy, 74.60.Jg

## I. INTRODUCTION

A central feature of the family of the high  $T_c$  cuprate superconductors is the weak coupling between planes which gives rise to very high conduction anisotropy in both the normal and superconducting states. It is also responsible for the richness of the phase diagram of vortices in a magnetic field and the fact that the vortices are not well pinned except in the low temperature vortex solid phase. They are usually modeled by discrete superconducting sheets parallel to the *ab* crystallographic plane weakly coupled together in the *c*-direction by extended Josephson junctions<sup>1</sup>. One of the more obvious experimental probes of pinning in this phase is to look at the  $V$ - $I$  response for currents which take one into the resistive régime where the vortices are dislodged. To interpret these measurements however it is very important to know about the current and voltage distribution. The present note investigates the current and potential distributions at low temperature in a field aligned with the *c*-axis at currents where breakdown occurs. One of the important points is that at first sight the physically unrelated *c*-axis and *ab*-plane resistive breakdowns interact to radically alter the current distribution, critical current and dynamic resistance. Not only does the voltage response along an *ab*-plane into which the current is injected and withdrawn (the “*ab* configuration” of Fig. 1) show features of the Josephson junctions between planes, but also the response to current injection and withdrawal on opposing *ab*-planes (the “*c* configuration” of Fig. 1) shows features of breakdown in the *ab*-plane. One manifestation is that the threshold current in the *ab* configuration on BSCCO single crystals<sup>2</sup> shows the same temperature and preparation dependence as for the *c* configuration<sup>3</sup>. This brings up the immediate question as to who measures what and does one measure what one thinks, but beyond that what do the results mean?

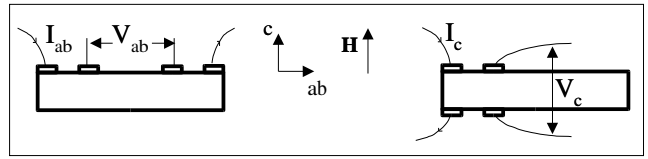


FIG. 1: *ab* and *c* contact configurations.

## II. EXPERIMENTAL TECHNIQUE

Our samples are thin monocrystalline platelets with the *c*-axis perpendicular to the face, all of which gave qualitatively the same results for similar contact configurations. We show here the results on three samples with differing contact configurations. The sizes of samples *A*, *B*, and *C* are about  $2 \times 0.35 \times 0.005 \text{ mm}^3$ ,  $1.1 \times 0.3 \times 0.002 \text{ mm}^3$  and  $0.7 \times 0.5 \times 0.005 \text{ mm}^3$ . They were all fabricated by a melt cooling technique<sup>4,5</sup>. The critical temperatures were between 88 and 90 K with a transition width of about 2 K at zero field. The anisotropy coefficient estimated from normal state resistivities were  $\gamma_n \approx 500$  with  $\rho_{ab} \approx 100 \mu\Omega\text{cm}$  at 90 K. In the case of samples *A* and *B*, electrical contact was made by bonding 25  $\mu\text{m}$  gold wires with silver epoxy fired at 900 K. For sample *C* the contacts were made by depositing silver on a lithographically defined area using a lift-off technique and heat treating at 700 K for 1000 s. In all cases the contact resistance was less than 3  $\Omega$ . The sample was mounted flat against a 7 mm diameter 0.5 mm thick sapphire disk with silicone grease to ensure the thermal homogeneity and mechanical freedom and placed in the bore of a superconducting magnet with the field along the *c*-direction, the sample and disk being surrounded by exchange gas and the temperature being electronically regulated. The  $V$ - $I$  characteristics were measured by a symmetrised differential four-point

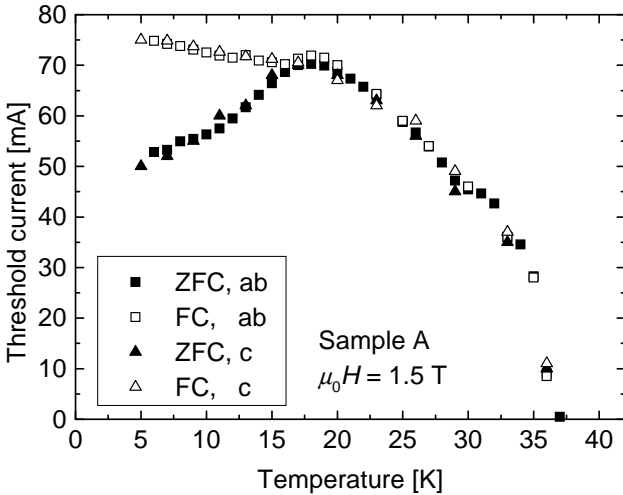


FIG. 2: Temperature dependence of the threshold current with *ab* and *c* contact configurations on the same sample.

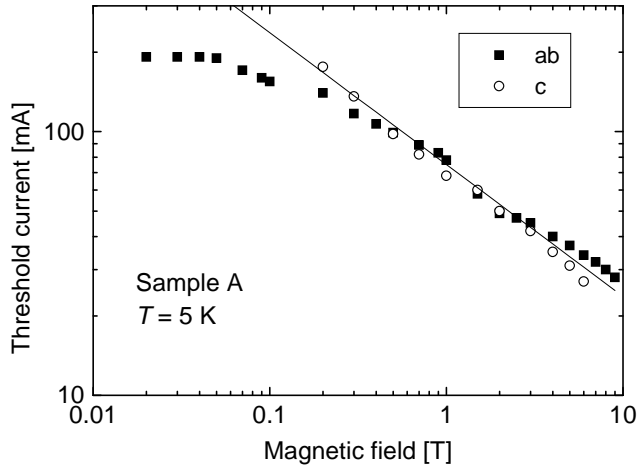


FIG. 3: Magnetic field dependence of the threshold current with both contact configurations on the same sample. The solid line shows  $H^{-1/2}$ .

technique using 25  $\mu$ s triangular pulses of maximum amplitude  $10 \text{ mA} < I_m < 350 \text{ mA}$  and repetition time 0.1 s (see Ref. 2 for further technical details).

### III. EXPERIMENTAL RESULTS

The first two samples were contacted to be able to measure in both *ab* and *c* configurations on the same sample at the same time. Fig. 2 shows the temperature dependence of the threshold current for sample *A* both for current applied along an *ab* surface or from one such surface to the other along the *c*-direction. The sample was prepared in two different ways: field cooled (FC), where the field is applied above  $T_c$  and the sample cooled at constant field to the lowest measuring tem-

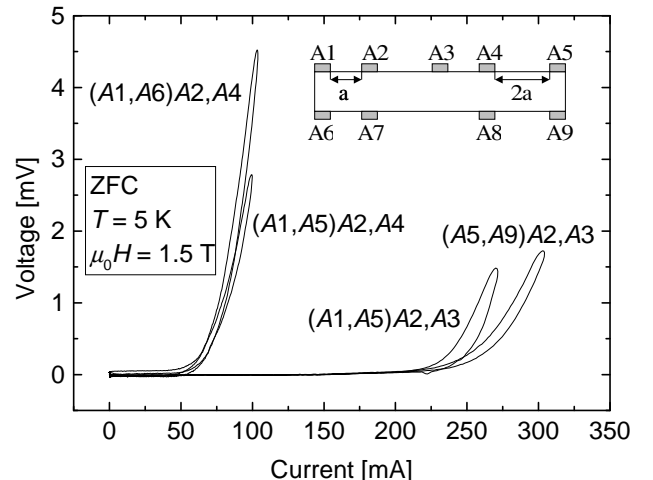


FIG. 4: *V*-*I* curves measured on sample *A*. The letters on the *V*-*I* curves refer to the contacts used: the first pair in brackets denote the current contacts and the last two the potential contacts. The insert shows the contact configuration.

perature, subsequent measurements being made on increasing the temperature at the same field, and zero field cooled (ZFC) where the system is cooled in zero field from above  $T_c$  to the lowest temperature before applying the field and making measurements at sequentially higher temperatures at the same field. The “*ab* configuration” measurements refer to the potential drop between contacts (*A*2, *A*4) for current injected at *A*1 and withdrawn from *A*5. The “*c* configuration” refers to the potential measured across (*A*2, *A*7) for current passed through (*A*1, *A*6). The threshold currents show the same temperature and preparation dependence in both configurations. Fig. 3 shows the magnetic field dependence in the same contact configurations for ZFC preparation at 5 K on increasing the field. Below 0.2 T the threshold for the *c* configuration was too high to measure, but at higher fields both configurations were measurable and were found to follow the same field dependence approximately  $H^{-1/2}$ . Surprisingly not only are the temperature and field dependences of the threshold current in the two configurations the same, but so are the actual values. This remarkable fact led us to look in more detail with the following experiment.

We use three potential contacts (*A*2, *A*3, *A*4) on the top layer and two (*A*7, *A*8) on the bottom. The contact *A*2 is half as far away from the left current contact *A*1 as is the contact *A*4 from the right hand current contact *A*5, while *A*3 is midway between the two current contacts. If we apply the current between contacts *A*1 and *A*5 (*ab*-direction) we measure a much lower threshold current between *A*2 and *A*4 than between *A*3 and *A*4 (see Fig. 4). On the other hand we find almost the same *V*-*I* curve on the *ab* potential contacts (*A*2, *A*4) with the current applied in the *c*-direction through contacts (*A*1, *A*6) as for an *ab* current through (*A*1, *A*5); similarly

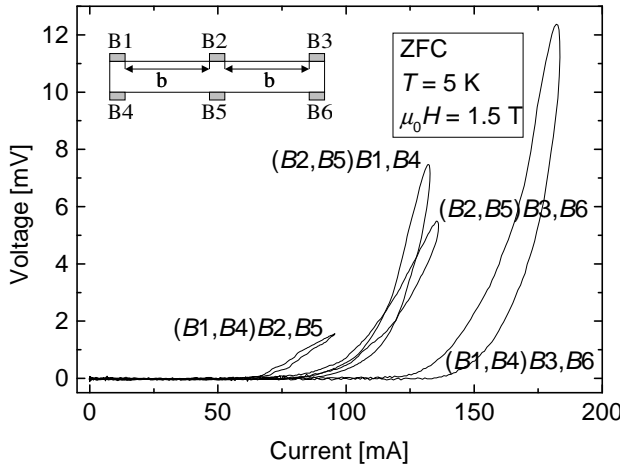


FIG. 5:  $V$ - $I$  response of sample  $B$ . The labelling convention is as before.

the  $V$ - $I$  across  $(A_3, A_4)$  is the same for  $ab$ -directed current through  $(A_2, A_4)$  or for  $c$ -directed current through  $(A_5, A_9)$ .

These results led us to experiment with the contact configuration of sample  $B$  illustrated in Fig. 5 where we drove the current through the  $c$ -direction and also measured the voltage drop across that direction. On pushing the current through  $(B_1, B_4)$  the  $V$ - $I$  characteristic measured across  $(B_2, B_5)$  shows a threshold current which is about half that measured across contacts  $(B_3, B_6)$ . On the other hand, if we put the current through the middle contacts  $(B_2, B_5)$  we find the same threshold at either of the two end potential contacts  $(B_1, B_4)$  or  $(B_3, B_6)$  with a value intermediate between the previous two.

To have more direct information about the shape of the front with depth, we prepared the third sample  $C$  as in Fig. 6 with a lithographically defined terrace argon ion etched along the length of one  $ab$  face to a depth of 220 nm. The upper part of the face was also argon ion etched to avoid any difference in surface pinning between it and the terrace, the width of which was restricted to a small fraction of the total width to minimise the effect of current spread as the distribution attains the depth of the terrace. The contacts were accurately aligned between the two levels by an electron beam masking microscope. On a control sample with the same contact configuration but with no the terrace, the  $V$ - $I$  response on contacts  $(C_2, C_3)$  gave the same values of the threshold current and dynamic resistance as contacts  $(C_5, C_6)$ , themselves very similar to those for the top contacts of the terraced sample.

Sending an  $ab$ -directed current through contacts  $(C_1, C_4)$  on the upper part of the face, we measured the potential drop across  $(C_2, C_3)$  on the upper part and across  $(C_5, C_6)$  on the step. The threshold current for the terrace contacts is considerably higher than for the corresponding top contacts: about 25 mA and 10 mA

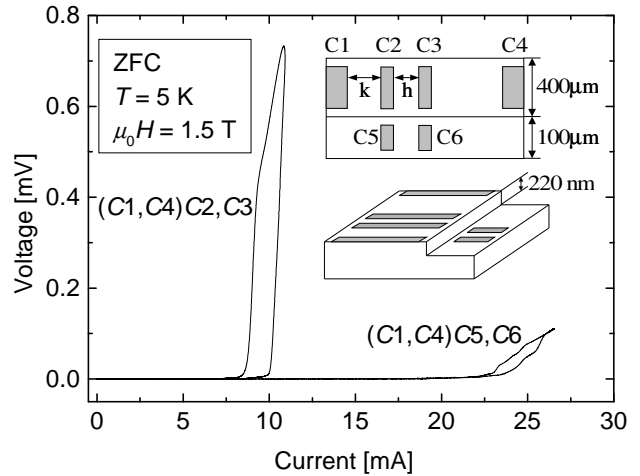


FIG. 6:  $V$ - $I$  curves of sample  $C$ . The dimensions  $k$  and  $h$  are 125 and 75  $\mu\text{m}$ , respectively.

respectively.

#### IV. INTERPRETATION OF EXPERIMENTAL RESULTS

All these observations are consistent with the idea of a resistive front moving progressively outward from the current contacts as illustrated in Fig. 7. Also, it seems that the position of the front depends only on the magnitude of the current injected and is independent of its ultimate destination if one is to account for the identical  $V$ - $I$  response on, for example, the potential contact pair  $(A_2, A_4)$  independently of whether the current is withdrawn on the same face  $(A_1, A_5)$  or the opposite face  $(A_1, A_6)$ . Similarly for the potential pair  $(A_3, A_4)$  for current through  $(A_5, A_1)$  or  $(A_5, A_9)$ . The difference between the values of the threshold current measured on  $(A_2, A_4)$  and  $(A_3, A_4)$  contact pairs is accounted for by the distances of the potential contact from the nearest current contact ( $A_2$  from  $A_1$  or  $A_5$  from  $A_6$ ). In these experiments, the fronts did not attain contact  $A_3$  which remained at the potential of the resistanceless region. The triangular form is schematic, but some justification for such a form is presented below.

Fig. 8 represents how the resistive front is imagined to progress in the experiment with sample  $B$  when the current is run through the  $c$ -direction. Here too the lower threshold current was obtained for potential pair  $(B_2, B_5)$  nearest the current contacts. The resistive front from current contacts  $(B_1, B_4)$  attains  $(B_2, B_5)$  before  $(B_3, B_6)$ . When the current was run through the middle of the sample by  $(B_2, B_5)$  the injected current is divided between two directions with a corresponding reduction in current density so that the voltage drop appears at higher current for the same distance and gives the same response at both ends. Fig. 9 represents the fronts for

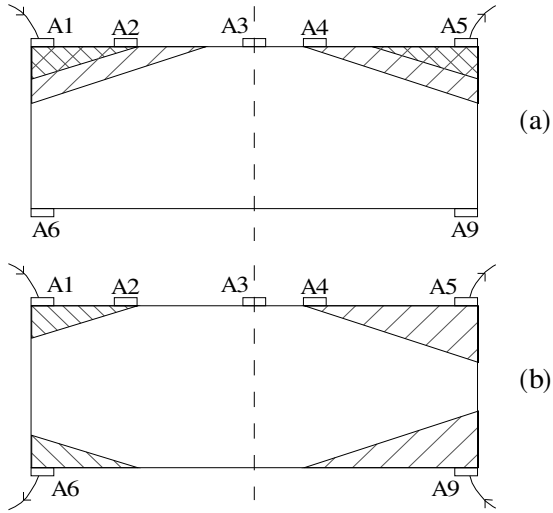


FIG. 7: Propagation of the resistive front in sample *A* with current directed in the (a) *ab* (*A*1, *A*5) and (b) *c* (*A*1, *A*6) or *c* (*A*5, *A*9) directions.

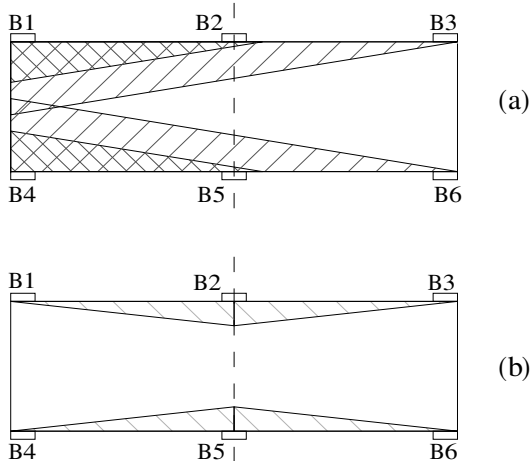


FIG. 8: Propagation of the resistive front with a *c*-directed current in sample *B*. The current was driven through (a) (*B*1, *B*4) contacts near one end of the sample (b) (*B*2, *B*5) at the middle of the sample.

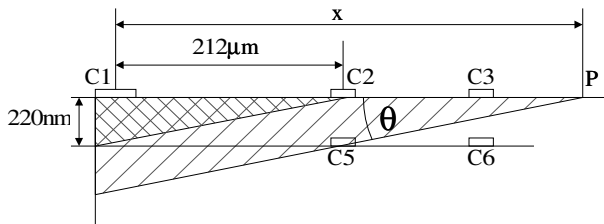


FIG. 9: Propagation of the resistive front through contact *C*5 which is on the etched step of sample *C*.

the experiment with the terraced sample. The front is defined by the current density reaching threshold for resistive breakdown in each principal direction simultaneously (*ab*-plane and *c*-direction) and the integral of the threshold current density crossing the front is just the total current. If the front does not change geometrical form with current amplitude its dimensions increase linearly with the current. Then knowing the distance from the nearest current contact and the depth of the terrace, the threshold current values for the upper and step contacts allow us to evaluate the angle between the face and the line defined by the points where the front pierces the upper and terrace levels (for a simple wedge, the wedge angle). The result, which we can expect to be related to the anisotropy, is  $\Theta = 0.7 \times 10^{-3}$  rad.

In the normal state typical anisotropy factors  $\gamma_n \approx 500$  indicate a current penetration depth of about  $\ell_c \approx \ell_{ab}/\gamma \approx 1 \mu\text{m}$  for a distance  $\ell_{ab} \approx 1 \text{ mm}$  between *ab* current contacts<sup>6</sup>. In the superconducting phase, experiments<sup>7</sup> on mesa structures of BSCCO have shown a Josephson current reduced by a factor of about 30 with a proportionally enhanced low current resistive slope over what is expected on the usual Ambegaokar-Baratoff<sup>8</sup> relation with the high current resistance. This has been attributed to the *d*-wave nature of the order parameter. This already enhances the anisotropy by a factor of  $\sqrt{30}$  over the normal state, but if one also considers the effect of phase fluctuations across the Josephson junction<sup>9</sup>, another factor of  $\langle \cos \varphi_{i,i+1} \rangle^{-1/2}$  should be incorporated into  $\gamma_s$ . This latter factor has been variously estimated as being between about  $10^{-2} - 10^{-1}$ , leading to an estimate for the anisotropy parameter in the superconducting phase  $3 \times 10^4 < \gamma_s < 3 \times 10^5$ . Current penetration in the superconducting phase is governed by a combination of London screening and anisotropy, both of which act to limit the penetration; in the absence of London screening, the equation governing the current penetration is the same as in the normal state except that the argument of the Laplacian is the superconductor phase rather than the electrical potential which, with the values estimated above, would give a penetration depth  $p$  in the middle of the sample  $2 < p < 20 \text{ nm} \ll \lambda_{ab} \simeq 200 \text{ nm}$ . The anisotropy factor  $\gamma_{rs}$  of the resistive superconductor regime is presumably enhanced by another factor  $(H_{c2}/B)^{1/2} \sim 10$  if vortex flow follows the Bardeen-Stephen<sup>10</sup> rule. Current penetration in the superconducting phase of BSCCO is thus always dominated by the anisotropy for short samples like ours.

This leads us to suggest a scenario where the current injected from an *ab* surface contact is confined by anisotropy to a penetration depth  $\ell_{ab}/\gamma_s$  with consequent enhancement of the current density. When the current density attains the critical value for either  $J_c$  or  $J_{ab}$ , the current distribution is modified until both reach their breakdown values and the sample is resistive on one side and non-resistive on the other side of a front which advances out from the current injection point as the current is increased. Very probably, its shape is fixed by the **E-J**

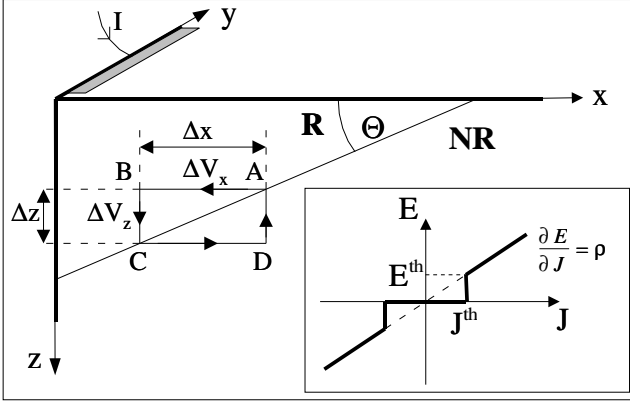


FIG. 10: The wedge angle of the resistive front; **R** denotes the resistive side, **NR** the non resistive side.  $\oint \mathbf{E} d\ell = 0$  for loop ABCD where A and C are on the interface and  $\mathbf{E} = 0$  over the segment CDA in the non resistive superconductor.  $\mathbf{E} = -\nabla V$  and  $\Delta V_x$  and  $\Delta V_z$  are the potential differences between A and B and between B and C respectively. The insert shows the hypothesis for the form of the **E-J** relationships along the principal axes.

response around the breakdown values (vortex depinning and Josephson junction behaviour) and moves away from the contact linearly with the current. As the apex of the front attains successive voltage contacts, they display a potential drop with respect to the portion of the sample which has remained in the non resistive state. We note that if the shape of the front is determined uniquely by the **E-J** response, its position depends only on the contact from which it originates and the magnitude of the current injected.

As indicated earlier, the shape of the wedge may be a simple triangle. Because  $\nabla \times \mathbf{E} = 0$  should be satisfied through the resistive–non resistive interface (Fig. 10), this interface can be neither everywhere parallel nor everywhere perpendicular to the *c*-axis. Minimum conditions for this are  $t/\ell < J_c^{\text{th}}/J_{ab}^{\text{th}} < \ell/t$  where violating the left hand inequality corresponds to sole *ab* breakdown (film) and the right hand to sole *c* breakdown (mesa) with corresponding uniformity of current density on the resistive side<sup>11</sup>. In our samples both *ab* and *c* breakdown appear simultaneously and the *V-I* response in either configuration contains both *c* and *ab* features. The simple analysis illustrated in Fig. 10 considers a segment of a resistive–non resistive interface making a local angle  $\Theta$  with the *ab*-plane in a region of simultaneous *ab* and *c* breakdown. The vanishing curl of the electric field means we can represent it by a scalar potential  $V(\mathbf{r})$  which we choose to be zero on the non resistive side of the interface. Following the loop in the figure:

$$\Delta V_x + \Delta V_z = (\partial V / \partial z) \Delta z + (\partial V / \partial x) \Delta x = 0 \quad (1)$$

Now if we had a simple **E-J** relation on the resistive side

of the form shown in the inset:

$$-\frac{\partial V}{\partial x} = \pm E_{ab}^0 + \rho'_{ab}(J_x \mp J_{ab}^{\text{th}}); J_x \gtrless \pm J_{ab}^{\text{th}} \quad (2)$$

$$-\frac{\partial V}{\partial z} = \pm E_c^0 + \rho'_c(J_z \mp J_c^{\text{th}}); J_z \gtrless \pm J_c^{\text{th}} \quad (3)$$

where  $\rho'_{ab}$  and  $\rho'_c$  are the dynamic resistivities in the *ab* and *c*-direction in the superconductive state beyond breakdown, the angle is given by

$$\tan \Theta = \Delta z / \Delta x = E_{ab}^0 / E_c^0 \quad (4)$$

Making the reasonable order of magnitude estimate that  $E_{ab}^0 \sim \rho'_{ab} J_{ab}^{\text{th}}$  and  $E_c^0 \sim \rho'_c J_c^{\text{th}}$  the angle is related to the anisotropy by

$$\tan \Theta \approx \frac{\rho'_{ab}}{\rho'_c} \frac{J_{ab}^{\text{th}}}{J_c^{\text{th}}} = \gamma_{rs}^{-2} \frac{J_{ab}^{\text{th}}}{J_c^{\text{th}}}. \quad (5)$$

This model predicts a constant angle and a simple wedge form dependent only on the **E-J** relationship in the superconductor resistive state. The position of the front is then dependent only on the magnitude and is independent of the ultimate destination of the current passing through the interface into the non resistive portion of the superconductor. Also the threshold current measured for contacts on the surface is given by  $I^{\text{th}} = w(dJ_{ab}^{\text{th}} + \ell J_c^{\text{th}}) = w\ell(J_{ab}^{\text{th}} \tan \Theta + J_c^{\text{th}})$  where *w*, *d* and *ℓ* are the width depth and length of the resistive wedge, the length being the distance to the nearest current injection point and the width that of the sample.

## V. SUMMARY

The experimental results confirm that for long thin samples *ab* - and *c* effects are always present simultaneously and that the *V-I* characteristics depend only on current magnitude, voltage contact position and nearest current injection point. In particular, they are independent of *ab* or *c* measurement configuration. The results are consistently accounted for by the idea of a resistive front advancing outwards from the current injection points, its form being independent of the ultimate destination of the current. We have made a measurement on the depth profile of the front and shown how a reasonable model accounts for its form being independent of the current destination and how it is related to the anisotropy.

## Acknowledgments

We take pleasure in acknowledging discussion with I. Tüttő, L. F. Kiss. We are grateful to L. Forró and to B. Keszei for supplying the crystals used in this study.

B. Sas and Á. Pallinger thank the Atomic Energy Commission for a Bursary to visit the Saclay laboratory. Research in Hungary has been supported by the grant

OTKA-T037976. We are grateful also for the support of the “BALATON” collaboration program of the French and Hungarian Foreign Affairs Ministries.

---

<sup>1</sup> W. E. Lawrence and S. Doniach, in *Proceedings of the XIIth Int. Conf. on Low Temp. Phys.*, edited by E. Kanda (Keigaku, Tokyo, 1971), p. 361.

<sup>2</sup> B. Sas, F. Portier, K. Vad, B. Keszei, L. F. Kiss, N. Hegeman, I. Puha, S. Mészáros, and F. I. B. Williams, Phys. Rev. B **61**, 9118 (2000).

<sup>3</sup> E. Rodríguez, M. F. Goffman, A. Arribre, F. de la Cruz, and L. F. Schneemeyer, Phys. Rev. Lett. **71**, 3375 (1993).

<sup>4</sup> B. Keszei, G. Szabó, J. Vandlik, L. Pogány, and G. Oszlányi, J. Less Common Metals **155**, 229 (1989).

<sup>5</sup> J. R. Cooper, L. Forró, and B. Keszei, Nature **343**, 444 (1990).

<sup>6</sup> R. Busch, G. Ries, H. Werthner, G. Kreiselmeyer, and G. Saemann-Ischenko, Phys. Rev. Lett. **69**, 522 (1992).

<sup>7</sup> L. N. Latyshev and T. Yamashita, Phys. Rev. Lett. **82**, 5345 (1999).

<sup>8</sup> V. Ambegaokar and A. Baratoff, Phys. Rev. Lett. **10**, 486 (1963).

<sup>9</sup> M. B. Gaifullin, Y. Matsuda, N. Chikumoto, J. Shimoyama, and K. Kishio, Phys. Rev. Lett. **84**, 2945 (2000).

<sup>10</sup> J. Bardeen and M. J. Stephen, Phys. Rev. **140**, A1197 (1965).

<sup>11</sup> F. London, *Superfluids* (Dover Publications, New York, 1960).